Environmental Science & Technology

Article

pubs.acs.org/est

Antagonistic Effects of Humic Acid and Iron Oxyhydroxide Grain-Coating on Biochar Nanoparticle Transport in Saturated Sand

Dengjun Wang,[†,‡] Wei Zhang,[§] and Dongmei Zhou*[,†]

[†]Key Laboratory of Soil Environment and Pollution Remediation, Institute of Soil Science, Chinese Academy of Sciences, Nanjing 210008, China

[§]Department of Plant, Soil and Microbial Sciences, Environmental Science and Policy Program, Michigan State University, East Lansing, Michigan 48824, United States

[‡]University of Chinese Academy of Sciences, Beijing 100049, China

Supporting Information

ABSTRACT: Biochar land application may result in multiple agronomic and environmental benefits (e.g., carbon sequestration, improving soil quality, and immobilizing environmental contaminants). However, our understanding of biochar particle transport is largely unknown in natural environments with significant heterogeneity in solid (e.g., patches of iron oxyhydroxide coating) and solution chemistry (e.g., the presence of natural organic matter), which represents a critical knowledge gap in assessing the environmental impact of biochar land application. Transport and retention kinetics of nanoparticles (NPs) from wheat straw biochars produced at two pyrolysis temperatures (i.e., 350 and 550 °C) were investigated in water-saturated sand columns at environmentally relevant concentrations of dissolved humic acid (HA, 0, 1, 5, and 10 mg L^{-1}) and fractional surface coverage of iron oxyhydroxide coatings on sand grains (ω, 0.16, 0.28, and 0.40). Transport of biochar NPs increased with increasing HA concentration, largely because of enhanced repulsive interaction energy between biochar NPs and sand grains. Conversely, transport of biochar NPs decreased significantly with increasing ω due to enhanced electrostatic attraction between negatively charged biochar NPs and positively charged iron oxyhydroxides. At a given ω of 0.28, biochar NPs were less retained with increasing HA concentration due to increased electrosteric repulsion between biochar NPs and sand grains. Experimental breakthrough curves and retention profiles were well described using a two-site kinetic retention model that accounted for Langmuirian blocking or random sequential adsorption at one site. Consistent with the blocking effect, the often observed flat retention profiles stemmed from decreased retention rate and/or maximum retention capacity at a higher HA concentration or smaller ω. The antagonistic effects of HA and iron oxyhydroxide grain-coating imparted on the mobility of biochar NPs suggest that biochar colloid transport potential will be dependent on competitive influences exerted by a number of environmental factors (e.g., natural organic matter and metal oxides).

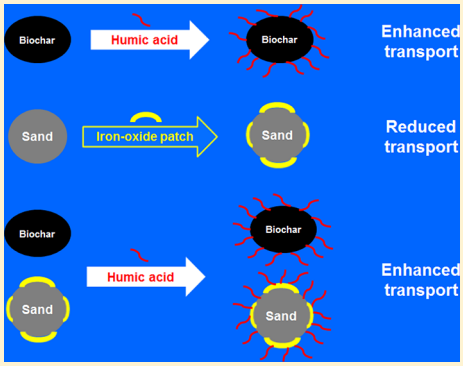

INTRODUCTION

Biochar is a carbon-bearing material that may be produced from pyrolysis of bioenergy feedstocks (e.g., grass, crop residue, and woody biomass) and agricultural wastes (e.g., manure) in the absence of oxygen and at relatively low carbonization temperature.[1] Recently, biochar is being considered as soil amendment to deliver multiple bioenergy, agronomic, and environmental benefits.[2−8] When applied to soils, biochar could become a net sink of atmospheric CO_2 due to its recalcitrant nature[2] and also reduce emission of greenhouse gases (e.g., CH_4 and NO_x),[9] thus mitigating climate change. Additionally, biochar land application could improve soil structure and fertility,[3] enhance fertilizer retention and use efficiency,[10] and increase crop production.[3] Moreover, biochar has increasingly been reported to effectively immobilize a variety of environmental contaminants (e.g., heavy metals, herbicides, PCBs, PAHs, and microbial pathogens).[5,11−15] Because of strong contaminant sorption capacity of biochars, facilitated transport of biochar-associated contaminants is possible under environmental conditions that favor mobilization of micrometer- or nanometer-sized biochar particles.[14,16] Unfortunately, to date little attention has been paid to the fate and transport of biochar colloids in soils and groundwater.

Natural organic matter (NOM) is ubiquitous in natural soils and aquatic environments and is mainly composed of humic substances such as humic acid (HA).[17] HA readily adsorbs onto a wide variety of solid surfaces, modifying their surface chemistry and thereby transport and adhesion properties.[18−30] For instance, HA was found to enhance the transport of colloids and nanoparticles (NPs) in granular media due to increased electrostatic or electrosteric repulsion induced by the

Received: December 29, 2012
Revised: April 17, 2013
Accepted: April 24, 2013
Published: April 24, 2013

Table 1. Electrokinetic Potentials of Biochar NPs and Sand Grains and XDLVO Parameters for NP-Sand Interaction Under Different HA Concentrations and Fractions of Iron Oxyhydroxide Coating (ω)

HA (mg L^{-1})	ω	EC[a] (μS cm^{-1})	pH	ζ_{WS350}[b] (mV)	ζ_{WS550}[c] (mV)	ζ_s[d] (mV)	$\Phi_{max\text{-}WS350}$[e] kT	$\Phi_{max\text{-}WS550}$[f] kT
0	0	25	6.9 ± 1.1[g]	−36.6[a,h]	−32.9[a]	−68.8[a]	133[e]	91.4[d]
1.0	0	24	6.9 ± 0.9	−43.4[b]	−37.9[b]	−69.6[a]	172[f]	113[e]
5.0	0	26	6.9 ± 1.2	−45.9[c]	−38.7[b]	−69.4[a]	185[f]	117[e]
10	0	26	7.0 ± 0.7	−46.8[c]	−39.3[b]	−69.2[a]	190[f]	119[e]
0	0.16	24	6.8 ± 1.2	−36.6[a]	−32.9[a]	−48.2[b]	98.1[c,d]	67.8[b,c]
0	0.28	25	6.9 ± 0.8	−36.6[a]	−32.9[a]	−37.7[c]	76.0[b]	53.2[b]
0	0.40	25	6.9 ± 0.5	−36.6[a]	−32.9[a]	−25.4[d]	47.0[a]	33.3[a]
1.0	0.28	26	6.9 ± 1.0	−43.4[b]	−37.9[b]	−39.2[c]	97.5[c]	66.3[b,c]
5.0	0.28	27	6.9 ± 1.0	−45.9[c]	−38.7[b]	−43.9[b]	117[d,e]	76.3[c]
10	0.28	24	6.9 ± 0.8	−46.8[c]	−39.3[b]	−45.1[b]	123[e]	79.8[c,d]

[a]Electrical conductivity. [b]ζ-potentials of WS350 and WS550 NPs, respectively. [c]ζ-potentials of WS350 and WS550 NPs, respectively. [d]ζ-potential of uncoated and iron oxyhydroxide-coated sand grains. [e]Primary energy barriers for WS350-water-sand and WS550-water-sand systems. [f]Primary energy barriers for WS350-water-sand and WS550-water-sand systems, respectively. [g]Mean value ± standard deviation. [h]Mean values followed by the same lowercase letters are not significantly different using Tukey's HSD test at $p < 0.05$.

HA macromolecules sorbed onto the surfaces of both colloids and collectors (e.g., soil grains).[18,20,21,27−29] Nonetheless, despite strong HA sorption on biochars,[31] the effect of HA on biochar NP mobility in granular media has not received any attention.

Additionally, variability in surface charge heterogeneity is common in natural soils, sediments, or groundwater aquifers, as a result of variations in soil texture and structure, recharge rate, aqueous and solid-phase geochemistry, and biological factors.[19,24,32] Surface charge heterogeneity is known to influence the deposition of colloids and NPs in granular media.[19,24,30,33−39] One of the most common sources for surface charge heterogeneity in natural aquatic environments is iron and aluminum oxyhydroxides[32,33,35,36] that are amphoteric minerals with relatively high points of zero charges (pH_{PZC}).[40] Often, the pH values in aquatic environments and aquifers are below the pH_{PZC} of iron (7.5) and aluminum oxyhydroxides (9.0), so these minerals acquire a net positive charge.[30,34,35,38,41] Because most biochars[42] and silica[28] exhibit a net negative charge at environmental pH, electrostatic conditions for biochar retention are expected to be "unfavorable" for negatively charged silica surfaces and "favorable" for positively charged patches of iron and aluminum oxyhydroxides. However, our previous studies confirmed that HA can significantly enhance the transport of hydroxyapatite NPs in saturated sand by masking surface charge heterogeneity of iron oxyhydroxides.[30,43] To the best of our knowledge, there have been no investigations concerning the effect of surface charge heterogeneity on the transport of biochar NPs in the presence of HA, i.e., the antagonistic effects of HA and iron oxyhydroxide grain-coating on the mobility of biochar NPs.

The overall objective of this study was to systematically investigate the role of HA concentration and iron oxyhydroxide grain-coating, both independently and in combination, in the transport and retention of biochar NPs in water-saturated sand.

MATERIALS AND METHODS

Biochar NP Suspensions, HA, and Granular Media. Wheat straw was utilized to prepare the biochars in this study. The biochars were produced under anaerobic condition at two pyrolysis temperatures (i.e., 350 and 550 °C), gently ground into powder form using an agate mortar, and then passed through a 150-μm sieve prior to use.[44] Hereafter the biochar samples were designated as WS350 and WS550, respectively. The procedure of preparing the biochar NP suspensions was similar to the one in our previous study.[44] Briefly, 7.5 g of biochar bulk powder was added to 500 mL of deionized (DI) water (18.2 MΩ cm, Millipore), gently stirred, and then sonicated in a water bath for 30 min to disperse the biochar stock suspension. The biochar NP suspension was generated by passing the biochar stock suspension through 100-nm pore size membranes (Kenker, USA). Afterward, the pH of the biochar NP suspensions was buffered to 6.9 (Table 1) using 0.1 mM $NaHCO_3$ solution. The concentration of the biochar NP suspension was determined spectrophotometrically (UV-3000D, Mapada Instrument Co., Ltd., Shanghai, China) at a wavelength of 221 nm (Supporting Information Figure S1) and was 300 ± 6.8 mg L^{-1}. A calibration curve was constructed by diluting a 600 mg L^{-1} biochar NP suspension (i.e., dispersing 0.060 g dry biochar NP powder into 100 mL of 0.1 mM $NaHCO_3$ solution at pH 6.9) over the range of 0−600 mg L^{-1}. The calibration curve had a high linearity (Figure S2).

HA (Sigma Aldrich, Germany) was used as model NOM in natural aqueous environments.[30] HA stock solution (100 mg L^{-1}) was prepared by introducing 100 mg of dry HA powder into 1 L of DI water.[30] A predetermined volume of HA stock solution was spiked into the above biochar NP suspension to generate the biochar suspension with the presence of 1, 5, or 10 mg L^{-1} HA, respectively. The biochar-free solutions of desired solution chemistry (Table 1) were used as background solutions in the column experiments. Quartz sand (purity >99.9%, 0.55−0.65 mm, and 0.60-mm median grain size, Sinopharm Chemical Reagent Co., Ltd., China) was used as model granular media. The sand was treated with H_2O_2 to remove organic matter and with sodium-dithionite to remove iron. Then the iron oxyhydroxide-coated sand was produced as described in detail in Supporting Information S1. Geochemically heterogeneous granular media were prepared by mixing portions of uncoated and iron oxyhydroxide-coated sand grains to achieve iron oxyhydroxide surface coverage (ω) of 0.16, 0.28, and 0.40 (Table 1), where ω is the fraction of the quartz sand coated by iron oxyhydroxide.

Characterization of Biochars and Granular Media. Physicochemical properties of the bulk biochars were closely examined in our previous study.[44] Selected biochar properties are given in Supporting Information Table S1. Zeta (ζ) potentials of WS350 and WS550 NPs and colloidal quartz sands (size <2 μm) in desired background solutions (Table 1)

were measured using a ZetaPlus analyzer (Brookhaven Instruments Corporation). Streaming potentials of iron oxyhydroxide-coated sand grains were determined by using a streaming potential analyzer (BI-EKA, Brookhaven Instruments Corporation). Detailed experimental procedures are given elsewhere.[37,38] Streaming potentials were converted to ζ-potentials using the Helmholtz-Smoluchowski equation.[45] This ζ-potential information was applied in conjunction with the extended Derjaguin−Landau−Verwey−Overbeek (XDLVO) theory to calculate total interaction energies of biochar NPs with the various granular media (S2). To assess HA sorption onto biochars and iron oxyhydroxide-coated sand grains, sorption isotherms of HA were obtained using a batch technique (S3).

Column Transport Experiments. Three sets of column experiments were conducted to examine the effects of HA and surface charge heterogeneity on the transport behaviors of biochar NPs in saturated granular media. The first set was designed to investigate the effect of environmentally relevant HA concentrations (0, 1, 5, and 10 mg L^{-1}) in uncoated quartz sand at pH 6.9 (Table 1). The second set was used to elucidate the influence of surface charge heterogeneity at pH 6.9. As mentioned above, surface charge heterogeneity was introduced into our model granular media by coating a fraction of the sand grains with iron oxyhydroxides (ω = 0.16, 0.28, and 0.40). A third set of experiments was intended to examine the effect of HA concentrations (0, 1, 5, and 10 mg L^{-1}) on the transport of biochar NPs in sand having a heterogeneous surface charge at fixed surface coverage of iron oxyhydroxides (ω = 0.28) (Table 1).

Saturated transport experiments were performed in triplicate using glass chromatography columns (2.6-cm in inner-diameter and 20.0-cm in length). The vertically oriented columns were wet-packed with tested granular media. In the experiments using iron oxyhydroxide-coated sand, the coated and uncoated sand grains were thoroughly mixed to ensure an even distribution in the column. Porosity of the packed columns was determined gravimetrically and varied between 0.38 and 0.42 (Table S2).

Column experiments were run in an upward flow mode using a peristaltic pump. Before initiating a transport experiment, the packed column was preconditioned with >10 pore volumes (PVs) of DI water at a flow rate of 0.50 mL min^{-1}. A nonreactive tracer experiment was then performed by injecting 1.0 PV of NaBr solution into the column and then eluted with 3.0 PVs of DI water (pH = 6.9). Column effluents were collected using a fraction collector. Bromide tracer concentrations were quantified by a bromide ion-selective electrode (PBr-1, Kangyi Instrument Co., Ltd., China). The column average pore-water velocity and dispersivity were obtained by fitting NaBr breakthrough curves (BTCs) to the one-dimensional form of the convection-dispersion equation (CDE) using the CXTFIT code.[46] Table S2 provides a summary of column transport properties for all experiments.

After the tracer test, two-phase transport experiments were performed: in phase 1, a stable biochar NP suspension at a concentration of 300 mg L^{-1} (C_0) with the desired background solution chemistry (Table 1) was introduced into the column for 3.0 PVs; and then in phase 2, another 3.0 PVs of biochar-free background solution were injected to flush any unattached biochar NPs remaining in the column. Effluent samples were collected by a fraction collector. The concentrations of biochar NPs in the effluents (C_i) were measured spectrophotometrically as described above. The BTCs were plotted as dimensionless concentrations (C_i/C_0) of biochar NPs as a function of PVs. Our preliminary experiments indicated that iron oxyhydroxide-coated sand at ω of 0.40 completely retained the injected biochar NPs at an input concentration of 60 mg L^{-1} (Figure S3). Therefore, a greater input biochar NP concentration (i.e., 300 mg L^{-1}) was selected in order to obtain the biochar BTCs suitable for subsequent transport modeling.

Following completion of each transport test, columns were sectioned into 10 layers of 2-cm segments. To determine the retention profiles (RPs) of biochar NPs, the biochar particles attached to collector grains in each fraction were subsequently re-entrained to extraction solutions. Note that DI water was the extractant in uncoated quartz sand experiments, whereas for the experiments with iron oxyhydroxide-coated sand, the extractant of 1.0 mM HCl was used in order to dissolve the iron oxyhydroxide coatings (2 h are needed).[44] The RPs were plotted as the normalized concentration (i.e., the quantity of the biochar NPs recovered in the sand, N_v, is divided by the quantity in a unit volume of the input biochar NP suspension per gram of dry sand) versus the distance from the column inlet. Mass balance was calculated by comparing the quantities of biochar in the effluent and retained in the sands to the initial amount injected into the column.

A one-dimensional form of the CDE with a two-site kinetic retention model was used to simulate the transport and retention of biochar NP in the column experiments. Details on the mathematical model, including governing equations, are given in S4.

Statistical Analysis. One-way ANOVA analysis was performed to identify statistically significant differences in measured parameters using the Tukey's Honestly Significant Different (HSD) test. All statistical analyses were conducted using SPSS 17.0, and the differences of means were considered significant at $p < 0.05$.

RESULTS AND DISCUSSION

Characteristics of Biochar NPs and Granular Media. Physicochemical properties of biochars WS350 and WS550 have been discussed in detail in our previous study[44] and will be briefly reiterated here. Compared to WS350 bulk powder, the WS550 had greater carbon content, alkalinity, hydrophobicity, and specific surface area as well as lower density of carboxylic and phenolic surface functional groups and subsequently less negative ζ-potentials (Table 1, Table S1, and ref 44). As shown in Table 1, the ζ-potentials of WS350 and WS550 NPs became more negative with increasing HA concentration, because of increased sorption of HA to biochars (Figure S4). Similarly, the negative ζ-potentials of the mixture of uncoated and iron oxyhydroxide-coated sand grains (ω = 0.28) generally increased in magnitude as HA concentration increased (Table 1), consistent with the reported results.[38] This observation may be attributed to the masking of the positively charged iron oxyhydroxide by the sorbed HA. The ζ-potentials for the mixtures of uncoated and iron oxyhydroxide-coated sand grains became significantly less negative as ω increased from 0 to 0.40 ($p < 0.05$, Table 1). Consistent with the previous findings,[35,37] the ζ-potential for the sand mixtures was the algebraic sum of the ζ-potential for the uncoated and iron oxyhydroxide-coated fractions (Figure S5), after correcting for ω.

HA Sorption to WS350 and WS550 Bulk Powders and Iron Oxyhydroxide-Coated Sand Grains. Sorption isotherms of HA to WS350 and WS550 bulk powders and iron

oxyhydroxide-coated sand grains are presented in Figure S4. Both Freundlich and Langmuir models performed equally well in describing HA sorption to WS350 and WS550 bulk powders (Figure S4 and Table S3). Nonetheless, the Langmuir model is not commonly used for heterogeneous and porous carbonaceous sorbents (e.g., activated carbon and biochar) because it presumes monolayer coverage and no sorbate intermolecular interaction.[31] The Freundlich model has been more often used to describe sorption of HA on activated carbons and biochars.[31,47] The Freundlich constants, K_F or "affinity coefficients", ranged from 105−2474 mg^{1-n} L^n kg^{-1}, whereas the Freundlich linearity parameters, n, ranged 0.3−0.713 (Table S3). A similar range of both K_F and n have also been reported for catechol and HA sorption on biochars.[31] The K_F of HA for WS550 was roughly 4 times larger than that of WS350 because WS550 had a higher specific surface area, hydrophobicity, micropore area, and micropore volume than WS350 (Table S1 and ref 44), which is consistent with the results of Kasozi et al.[31] However, the maximum sorption capacity (S_{max}) fitted by the Langmuir model for WS350 and WS550 was 17196 and 19813 mg kg^{-1} (Table S3), respectively. This negligible difference between the S_{max} values of the WS350 and WS550 bulk powders suggests that the Langmuir model cannot adequately capture the features of HA sorption on heterogeneous and porous biochars, because HA can strongly sorb onto biochar due to physical (e.g., physical entrapment) and/or chemical interactions (e.g., van der Waals interaction, hydrophobic interaction, $\pi-\pi$ interaction, and ligand exchange).[31,48]

Conversely, the Langmuir model provided a better description for HA sorption to iron oxyhydroxide-coated sand than the Freundlich model (Figure S4 and Table S3). The HA sorption isotherm showed an initial steep slope and reached a plateau at elevated equilibrium HA concentrations (Figure S4c, d), and the Freundlich model cannot capture this salient feature.[49] The Langmuir model has been more commonly used to describe sorption of humic substances to oxide surfaces, which has been attributed to anion exchange (electrostatic attraction), ligand exchange-surface complexation, hydrophobic interaction, entropic effect, hydrogen bonding, and cation bridging.[49,50] The maximum sorption capacity of HA on iron oxyhydroxide-coated sand was 329 mg kg^{-1}, more than 1 order of magnitude smaller than those of WS350 and WS550 bulk powders (Figure S4 and Table S3). This is partly due to a smaller specific surface area of the iron oxyhydroxide coating than these two biochar bulk powders (S1 and Table S1).

Effects of HA on Biochar NPs Mobility. Figure 1a,b presents the BTCs and RPs of WS350 NPs in uncoated quartz sand in the presence of 0, 1, 5, and 10 mg L^{-1} HA (pH = 6.9), whereas Figure 1c,d presents similar information for WS550 NPs. The corresponding mass recoveries of WS350 and WS550 NPs in the effluent and from the sand are shown in Table S2. Because virtually all (100−108%) of the injected biochar NPs were recovered, there is a high degree of confidence in the experimental procedure.

Both breakthrough of WS350 and WS550 NPs were at ∼0.90 PV and then gradually reached to a plateau at ∼2.0 PV. The BTCs were symmetrical and exhibited low degree of tailing, consistent with the results observed in our previous study.[44] Transport of WS350 NPs generally increased with increasing HA concentration (see M_{eff} in Table S2). A similar trend of increasing effluent mass recovery with increasing HA concentration was observed for the WS550 NPs (Figure 1c and Table S2). This is likely due to the increased electrostatic

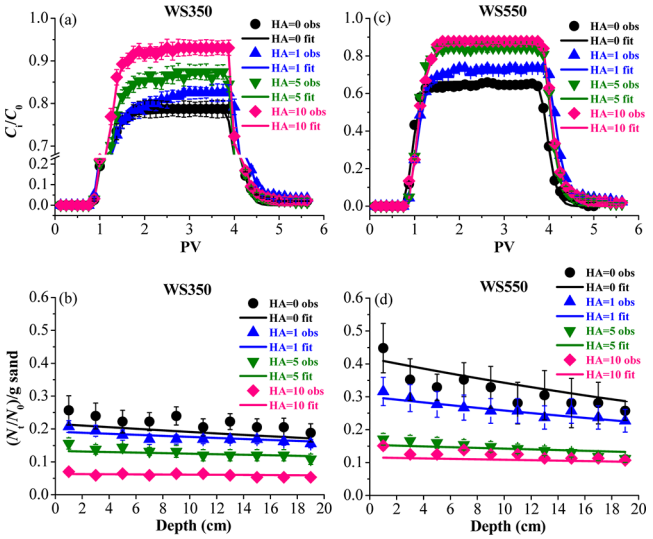

Figure 1. Measured and fitted BTCs (a, c) and RPs (b, d) for WS350 and WS550 NPs, respectively, under the HA concentrations of 0, 1, 5, and 10 mg L^{-1} in uncoated quartz sand (pH = 6.9). Fitted curves were obtained using the two-site kinetic retention model that assumed Langmuirian blocking on site 2. In (b, d) the normalized concentration (the quantity of the biochar NP recovered in the sand, N_t is divided by the quantity in a unit volume of the input biochar NP suspension) per gram of dry sand was plotted as a function of distance from the column inlet. Error bars represented the standard deviations in triplicate experiments.

or steric repulsions[18,20,21,27,29,30,38] between biochar NPs and sand grains at higher HA concentrations (Table 1). It should be mentioned that the symmetrical shape and absence of tailing in the nonreactive tracer BTC indicate that physical nonequilibrium processes (e.g., rate-limited mass transfer into immobile water regions and preferential flow paths)[51] did not exist in the packed columns (Figure S6a).

The breakthrough concentrations of WS350 NPs were always higher than those for WS550 NPs (Figure 1a,c and Table S2). This is partly due to the more negative ζ-potentials and hydrophilicity of WS350 NPs than those of WS550 NPs, which resulted in greater electrostatic and acid−base repulsions and subsequently greater total repulsive interaction energies between WS350 NPs and sand grains than those of WS550 NPs interacting with sand grains (Table 1 and ref 44). Although the sand was at least 99.9% quartz and had been thoroughly washed prior to the column tests, effluent mass recoveries of biochar NPs were still less than 100% (Figure 1a,c and Table S2). This is likely due to surface charge heterogeneity on the quartz grains (e.g., metal oxide patches),[30,52,53] surface roughness of the sand grains,[54] and enhanced colloid retention in low velocity regions.[41,55] Li et al. also suggested the existence of metal oxide patches on thoroughly cleaned quartz grains.[53]

In contrast with classical filtration theory[56] that predicts exponential profile with depth, the RPs for biochar NPs typically exhibited a somewhat uniform distribution with depth (i.e., a flat RP) (Figure 1b,d). It appeared that the RPs became flatter, and the biochar NP retention decreased at higher HA concentrations (Table S2). Similar RPs have been observed for carbonaceous fullerene (C_{60}) NPs in glass beads and Ottawa sands under unfavorable attachment conditions, which was attributed to saturating the maximum retention capacity that was determined by surface charge heterogeneity of the collector

dx.doi.org/10.1021/es305337r | Environ. Sci. Technol. 2013, 47, 5154−5161

grains.[51,53] Compared with our previous study performed at a biochar NP concentration of 200 mg L^{-1} and exhibited a hyperexponential RP,[44] the flat RP in this study was likely due to a high biochar NP input concentration (i.e., 300 mg L^{-1}). The high input concentration could quickly fill up the retention sites at the upper profile, which allows the biochar NP to migrate downward. Similar results of transforming hyperexponential RPs into flat RPs with increased input particle concentrations (Figure S7) were reported elsewhere.[57] Another possible explanation for the flat RPs is the blocking of suspended biochar NPs by previously deposited particles, as systematically elucidated by Tufenkji et al.[58] Thus, the transition from the straining-dominant retention at lower input concentrations[44] to the blocking-dominant retention at higher input concentrations warrants the incorporation of blocking function in the transport modeling.

The two-site kinetic retention model that assumes Langmuirian blocking on site 2 provided a good description for both BTCs and RPs of WS350 and WS550 NPs, respectively, under different HA concentrations ($R^2 \geq 0.994$, Table S4). It is hypothesized that the site 2 may be related to surface charge heterogeneity (e.g., metal oxide patches) of the sand grains due to irreversible attachment at this site. The values of S_{max2} and k_2 both decreased with increasing HA concentration. This is likely due to the reduced surface charge heterogeneity of sand grains and therefore the enhanced electrostatic and/or steric repulsions between biochar NPs and sand grains at higher HA concentrations, consistent with the previous studies.[18,20,21,27,29,30,38] As the Langmuirian blocking model could not be used in our earlier studies on biochar particle transport in porous media,[44,59] it was difficult to compare the fitted parameters in this study with those of our previous studies. Using the Langmuirian blocking model, Li et al.[53] and Wang et al.[51] obtained values of S_{max2} ranging from 0.15−0.56 (N_t/N_0) g^{-1} sand for fullerene NP suspensions (diameter = 92−95 nm, C_0 = 1.3−3.1 mg L^{-1} at 3.1 mM ionic strength) delivered at pore-water velocities of 0.08−0.58 cm min^{-1} in water-saturated quartz sands with 0.13−0.71 mm mean grain diameter,[51,53] which were much lower than these observed in this study performed at a pore-water velocity of 0.23 cm min^{-1} and ionic strength of 0.1 mM in quartz sands of 0.60-mm mean size (i.e., 1.94 and 10.0 (N_t/N_0) g^{-1} sand, for WS350 and WS550 NPs, respectively, at HA = 0 and ω = 0, Table S4). As the S_{max2} values are dependent on complex interplays of solution chemistry, flow hydrodynamics, and properties of colloids and collectors and generally increase with decreasing flow velocity, increasing solution ionic strength, decreasing colloid size, and increasing physical size and magnitude of heteogeneous surface charges,[51,53,60,61] it is difficult to compare the results from the studies performed under different experimental conditions. However, as flow velocity, sizes of NPs and sand grains, and sand surface property are comparable in these stuides, and the ionic strength in this study is much lower than those in Li et al.[53] and Wang et al.,[51] these factors are not likely to be responsible for the observed S_{max2} difference. Instead, the difference in surface properties of NPs is more likely to the cause, but the exact mechanism remains unknown without further study. The value of k_1 also decreased with increasing HA concentration. This observation suggests that mechanisms controlling biochar NP retention on reversible attachment site (site 1) are also sensitive to the HA concentration, consistent with the results in our previous study.[30]

Effect of Iron Oxyhydroxide Coating on Biochar NPs Mobility. Figure 2a,b and Figure 2c,d present the BTCs and

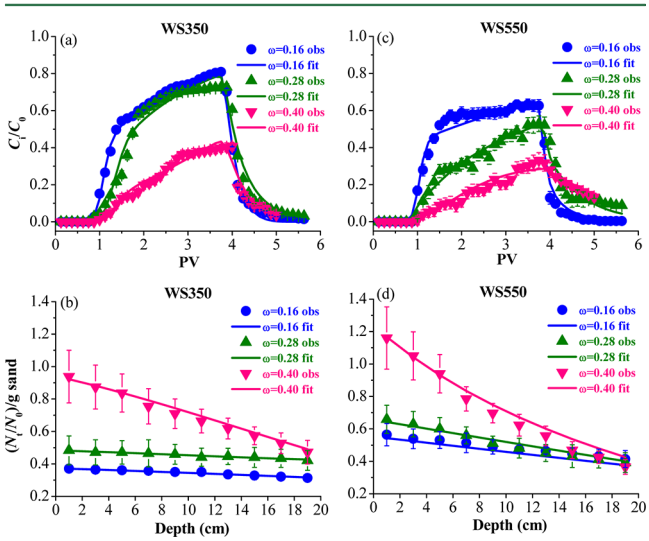

Figure 2. Measured and fitted BTCs (a, c) and RPs (b, d) for WS350 and WS550 NPs, respectively, under the iron oxyhydroxide coating fractions (ω, the fraction of the quartz grain surfaces coated by iron oxyhydroxide) of 0.16, 0.28, and 0.40 (HA = 0 and pH = 6.9). Fitted curves were obtained using the two-site kinetic retention model that assumed random sequential adsorption on site 2. Error bars represented the standard deviations in triplicate experiments.

RPs for WS350 and WS550 NPs, respectively, in various mixtures of uncoated and iron oxyhydroxide-coated sand grains (ω = 0.16, 0.28, and 0.40) in the absence of HA (pH = 6.9). Iron oxyhydroxide grain-coating had a substantial effect on the transport and retention of WS350 and WS550 NPs. Both WS350 and WS550 NPs broke through at progressively later times (see the tracer BTC for comparison, Figure S6b) and had lower amounts of biochar NPs in the effluent as ω increased. For instance, the mass recoveries of WS350 NPs were 69.0, 65.3, and 30.0%, respectively, when ω was 0.16, 0.28, and 0.40 (Table S2). A similar trend of decreasing effluent mass recovery with increasing ω was observed for WS550 NPs (Figure 2c and Table S2). These observations reflect the larger fraction of the surface area that is favorable (positively charged iron oxyhydroxide) for biochar NPs attachment at higher ω. Only after these favorable sites associated with the iron oxyhydroxide are occupied can substantial breakthrough start to occur. The gradual rising effluent concentration and the lack of effluent concentration plateau are the hallmark of blocking behavior in colloid and nanoparticle transport, suggesting decreasing rates of deposition with time.[30,34,35,39,62] For a given ω, the transport of WS350 NPs was always higher than WS550 NPs (Figure 2a,c and Table S2), similar to the results presented above.

The two-site kinetic retention model that assumes random sequential adsorption (RSA) on site 2 described both the BTCs and RPs well under the tested ω range (Figure 2 and Table S4). In general, the values of S_{max2} and k_2 tended to increase with ω. This trend is expected because S_{max2} is proportional to the fraction of the surface area favorable for attachment (e.g., iron oxyhydroxide coating).[30,33−35,39] The value of k_1 also increased with increasing ω. However, the value of k_{1d} decreased with increasing ω (Table S4). These observations suggest that biochar NP retention on reversible attachment site (site 1) is also sensitive to ω (i.e., decreased detachment with increasing

dx.doi.org/10.1021/es305337r | Environ. Sci. Technol. 2013, 47, 5154−5161

ω). As mentioned above, the values of S_{max2} in this study (Table S4) were much greater than those obtained by Li et al.[53] and Wang et al.[51] in uncoated quartz sand. However, the S_{max2} values (with the exception of WS550 NP at ω = 0.40) in our study were nearly 2−3 orders of magnitude smaller than the one (i.e., 1300 (N_t/N_0) g^{-1} sand for citrate-modified AgNP) reported by El-Badawy et al.[63] in ferrihydrite-coated quartz sand. This is likely due to the negatively charged citrate-AgNP can sorb onto the positively charged iron oxyhydroxide (i.e., ferrihydrite) through electrostatic attraction and inner sphere complexation ($-COOH^-$ of citrate with $Fe-OH^+$),[64] while the biochar NP can sorb onto the iron oxyhydroxide by means of electrostatic attraction only. Also, it is worth noticing that the Langmuirian model (S4) adequately described the experimental data in uncoated quartz sand (Figure 1 and Table S4), whereas the RSA model (S4) represented the experimental data better in iron oxyhydroxide-coated sand (Figure 2 and Table S4). This is likely due to the different contribution of the surface charge heterogeneity in colloid retention between these two models. Namely, the surface charge heterogeneity plays a relatively small role in colloid retention in the Langmuirian model, whereas it acts a predominant role in the RSA model (see S_{max2} in Table S4).[34,35]

Antagonistic Effects of HA and Iron Oxyhydroxide Coating on Biochar NPs Mobility. Figure 3a,b and Figure 3c,d present the BTCs and RPs of WS350 and WS550 NPs, respectively, under the HA concentrations of 0, 1, 5, and 10 mg L^{-1} at ω = 0.28 and pH = 6.9. HA had a significant impact on the biochar NPs transport and retention in the presence of iron oxyhydroxide grain-coating. The biochar NPs broke through at a progressively earlier time and, as expected, were subject to lower degree of attenuation (M_{eff} increased significantly from 65.3 to 78.8% and from 48.2 to 78.1% for WS350 and WS550 NPs, respectively, Table S2) as HA concentration increased from 0 to 10 mg L^{-1}. These observations were consistent with a quartz-dominated system (Figure 1) at lower ω and relatively higher concentrations of HA. Intriguingly, when only a minute amount of HA (1 mg L^{-1}) was added to the biochar NP suspensions, the slope of the rising limb of the BTCs was significantly increased. This was especially true for WS550 NPs due, in part, to much greater HA sorption on WS550 (Figure S4), thus greater electrosteric repulsion as explained below.[20,29,65,66] With increasing HA concentration, the ζ-potentials of biochar NPs, quartz grains, and iron oxyhydroxides became more negative (Table 1), because of increased HA sorption (Figure S4). Consequently, the energy barrier to retention in the primary minimum increased, resulting in less retention of biochar NPs. Also, steric repulsion invoked by HA coating on the biochar NPs and the sand grain surface would be enhanced with increasing HA concentrations because steric repulsion is proportional to the amount of HA sorption.[20,29,65,66] Enhanced steric repulsion, although not considered in the XDLVO calculations, would similarly result in lower biochar NP retention. The transport parameters estimated by the two-site kinetic retention model (Figure 3) were generally in agreement with the XDLVO energies. For instance, the values of k_1 and k_2 both decreased with increasing HA concentration (Table S4). These observations suggest that biochar NPs retention on both sites 1 and 2 was dependent on electrosteric interactions. Similar results were reported in our previous work.[30] Like the observations in the uncoated sand (Figure 1b,d), the biochar RPs became flatter at higher HA concentrations (Figure 3b,d). As elucidated earlier, this was likely due to the reduced retention rates at higher HA concentrations (Table S4). It is obvious that the presence of HA counteracted the enhanced biochar retention brought about by the iron oxyhydroxide coating, suggesting an antagonistic effect between these two common constituents (i.e., HA and iron oxyhydroxide coating) of natural aqueous environment (e.g., soils, sediments, and groundwater aquifer).

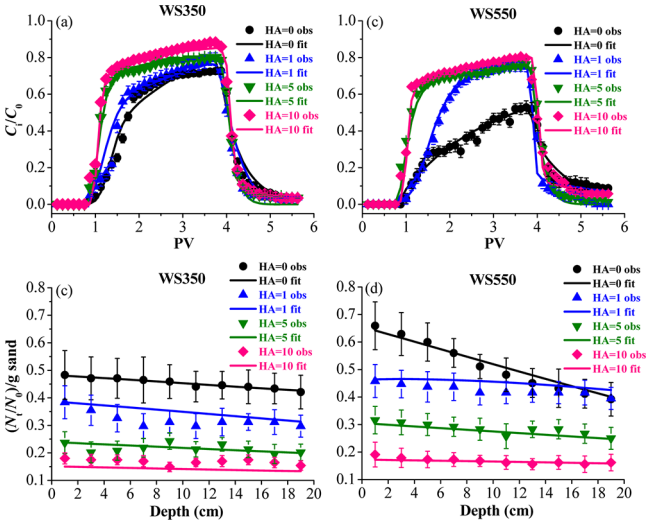

Figure 3. Measured and fitted BTCs (a, c) and RPs (b, d) for WS350 and WS550 NPs, respectively, under the HA concentration of 0, 1, 5, and 10 mg L^{-1} at ω = 0.28 (pH = 6.9). Fitted curves were obtained using the two-site kinetic retention model that assumed RSA on site 2. Error bars represented the standard deviations in triplicate experiments.

Environmental Implications. This study highlights several environmental implications for biochar land application. NOM ubiquitous in natural soils can significantly enhance biochar NP mobility in the environment. In particular, when the biochars are added to agricultural fields with applications of organic-rich animal manures, there may be a great potential for the mobilization of biochar particles and subsequently the facilitated transport of contaminants strongly adsorbed on the biochars, especially during rainfall events. While metal oxide (e.g., iron oxyhydroxide) commonly found in natural soils, sediments, and groundwater aquifers[32,36] may slow down the transport of biochar particles, NOM can effectively reduce this retardation effect. This study improved our understanding on the transport of biochar particles in saturated sand media in the presence of dissolved NOM and/or iron oxyhydroxide grain-coating, compared with the previous studies using model systems.[44,59] Nonetheless, natural soils and sediments vary in their texture, mineralogy, chemical compositions, and hydrologic regimes (saturated or unsaturated conditions), and the biochars may be land-applied in a variety of climatic and agricultural settings. Future research should focus on the transport of biochar particles and biochar-associated contaminants under more representative environmental conditions and agricultural practices.

■ ASSOCIATED CONTENT

Ⓢ Supporting Information

Details of the procedures involved in the properties of biochar and iron oxyhydroxide-coated sand, extended DLVO theory, sorption isotherm, transport model, model parameter, and mass

dx.doi.org/10.1021/es305337r | Environ. Sci. Technol. 2013, 47, 5154−5161

balance of column experiment. This material is available free of charge via the Internet at http://pubs.acs.org.

AUTHOR INFORMATION

Corresponding Author

*Phone: +86-25-86881180. Fax: +86-25-86881000. E-mail: dmzhou@issas.ac.cn.

Notes

The authors declare no competing financial interest.

ACKNOWLEDGMENTS

We thank three anonymous reviewers for their constructive and valuable comments. Funding was provided by the Specific Research on Public Service of Environmental Protection in China (201009009).

REFERENCES

(1) Lehmann, J.; Joseph, S. *Biochar for Environmental Management: Science and Technology*; Earthscan: London and Sterling, VA, 2009.

(2) Lehmann, J. A handful of carbon. *Nature* **2007**, *447* (7141), 143−144.

(3) Lehmann, J. Bio-energy in the black. *Front. Ecol. Environ.* **2007**, *5* (7), 381−387.

(4) Atkinson, C. J.; Fitzgerald, J. D.; Hipps, N. A. Potential mechanisms for achieving agricultural benefits from biochar application to temperate soils: a review. *Plant Soil* **2010**, *337* (1−2), 1−18.

(5) Jones, D. L.; Edwards-Jones, G.; Murphy, D. V. Biochar mediated alterations in herbicide breakdown and leaching in soil. *Soil Biol. Biochem.* **2011**, *43* (4), 804−813.

(6) Laird, D. A. The charcoal vision: a win-win-win scenario for simultaneously producing bioenergy, permanently sequestering carbon, while improving soil and water quality. *Agron. J.* **2008**, *100* (1), 178−181.

(7) Sohi, S. P. Carbon storage with benefits. *Science* **2012**, *338*, 1034−1035.

(8) Sparrevik, M.; Field, J. L.; Martinsen, V.; Breedveld, G. D.; Cornelissen, G. Life cycle assessment to evaluate the environmental impact of biochar implementation in conservation agriculture in Zambia. *Environ. Sci. Technol.* **2013**, *47* (3), 1206−1215.

(9) Spokas, K. A.; Koskinen, W. C.; Baker, J. M.; Reicosky, D. C. Impacts of woodchip biochar additions on greenhouse gas production and sorption/degradation of two herbicides in a Minnesota soil. *Chemosphere* **2009**, *77* (4), 574−581.

(10) Liang, B.; Lehmann, J.; Solomon, D.; Kinyangi, J.; Grossman, J.; O'Neill, B.; Skjemstad, J. O.; Thies, J.; Luizao, F. J.; Petersen, J.; Neves, E. G. Black carbon increases cation exchange capacity in soils. *Soil Sci. Soc. Am. J.* **2006**, *70* (5), 1719−1730.

(11) Cao, X. D.; Ma, L. N.; Gao, B.; Harris, W. Dairy-manure derived biochar effectively sorbs lead and atrazine. *Environ. Sci. Technol.* **2009**, *43* (9), 3285−3291.

(12) Chen, B. L.; Zhou, D. D.; Zhu, L. Z. Transitional adsorption and partition of nonpolar and polar aromatic contaminants by biochars of pine needles with different pyrolytic temperatures. *Environ. Sci. Technol.* **2008**, *42* (14), 5137−5143.

(13) Hale, S. E.; Hanley, K.; Lehmann, J.; Zimmerman, A. R.; Cornelissen, G. Effects of chemical, biological, and physical aging as well as soil addition on the sorption of pyrene to activated carbon and biochar. *Environ. Sci. Technol.* **2011**, *45* (24), 10445−10453.

(14) Uchimiya, M.; Lima, I. M.; Klasson, K. T.; Chang, S. C.; Wartelle, L. H.; Rodgers, J. E. Immobilization of heavy metal ions (Cu^{II}, Cd^{II}, Ni^{II}, and Pb^{II}) by broiler litter-derived biochars in water and soil. *J. Agric. Food Chem.* **2010**, *58* (9), 5538−5544.

(15) Abit, S. M.; Bolster, C. H.; Cai, P.; Walker, S. L. Influence of feedstock and pyrolysis temperature of biochar amendments on transport of *Escherichia coli* in saturated and unsaturated soil. *Environ. Sci. Technol.* **2012**, *46* (15), 8097−8105.

(16) Kookana, R. S.; Sarmah, A. K.; Van Zwieten, L.; Krull, E.; Singh, B. Biochar application to soil: agronomic and environmental benefits and unintended consequences. *Adv. Agron.* **2011**, *112*, 103−143.

(17) Amirbahman, A.; Olson, T. M. Deposition kinetics of humic matter-coated hematite in porous media in the presence of Ca^{2+}. *Colloids Surf., A* **1995**, *99* (1), 1−10.

(18) Kretzschmar, R.; Robarge, W. P.; Amoozegar, A. Influence of natural organic-matter on colloid transport through saprolite. *Water Resour. Res.* **1995**, *31* (3), 435−445.

(19) Ryan, J. N.; Elimelech, M. Colloid mobilization and transport in groundwater. *Colloids Surf., A* **1996**, *107*, 1−56.

(20) Kretzschmar, R.; Hesterberg, D.; Sticher, H. Effects of adsorbed humic acid on surface charge and flocculation of kaolinite. *Soil Sci. Soc. Am. J.* **1997**, *61* (1), 101−108.

(21) Kretzschmar, R.; Sticher, H. Transport of humic-coated iron oxide colloids in a sandy soil: influence of Ca^{2+} and trace metals. *Environ. Sci. Technol.* **1997**, *31* (12), 3497−3504.

(22) Kretzschmar, R.; Sticher, H. Colloid transport in natural porous media: influence of surface chemistry and flow velocity. *Phys. Chem. Earth* **1998**, *23* (2), 133−139.

(23) Kretzschmar, R.; Holthoff, H.; Sticher, H. Influence of pH and humic acid on coagulation kinetics of kaolinite: a dynamic light scattering study. *J. Colloid Interface Sci.* **1998**, *202* (1), 95−103.

(24) Kretzschmar, R.; Borkovec, M.; Grolimund, D.; Elimelech, M. Mobile subsurface colloids and their role in contaminant transport. *Adv. Agron.* **1999**, *66*, 121−193.

(25) Chen, K. L.; Elimelech, M. Influence of humic acid on the aggregation kinetics of fullerene (C_{60}) nanoparticles in monovalent and divalent electrolyte solutions. *J. Colloid Interface Sci.* **2007**, *309* (1), 126−134.

(26) Hyung, H.; Fortner, J. D.; Hughes, J. B.; Kim, J. H. Natural organic matter stabilizes carbon nanotubes in the aqueous phase. *Environ. Sci. Technol.* **2007**, *41* (1), 179−184.

(27) Keller, A. A.; Wang, H. T.; Zhou, D. X.; Lenihan, H. S.; Cherr, G.; Cardinale, B. J.; Miller, R.; Ji, Z. X. Stability and aggregation of metal oxide nanoparticles in natural aqueous matrices. *Environ. Sci. Technol.* **2010**, *44* (6), 1962−1967.

(28) Petosa, A. R.; Jaisi, D. P.; Quevedo, I. R.; Elimelech, M.; Tufenkji, N. Aggregation and deposition of engineered nanomaterials in aquatic environments: role of physicochemical interactions. *Environ. Sci. Technol.* **2010**, *44* (17), 6532−6549.

(29) Morales, V. L.; Zhang, W.; Gao, B.; Lion, L. W.; Bisogni, J. J.; McDonough, B. A.; Steenhuis, T. S. Impact of dissolved organic matter on colloid transport in the vadose zone: deterministic approximation of transport deposition coefficients from polymeric coating characteristics. *Water Res.* **2011**, *45* (4), 1691−1701.

(30) Wang, D. J.; Bradford, S. A.; Harvey, R. W.; Gao, B.; Cang, L.; Zhou, D. M. Humic acid facilitates the transport of ARS-labeled hydroxyapatite nanoparticles in iron oxyhydroxide-coated sand. *Environ. Sci. Technol.* **2012**, *46* (5), 2738−2745.

(31) Kasozi, G. N.; Zimmerman, A. R.; Nkedi-Kizza, P.; Gao, B. Catechol and humic acid sorption onto a range of laboratory-produced black carbons (biochars). *Environ. Sci. Technol.* **2010**, *44* (16), 6189−6195.

(32) Ryan, J. N.; Gschwend, P. M. Effect of iron diagenesis on the transport of colloidal clay in an unconfined sand aquifer. *Geochim. Cosmochim. Ac.* **1992**, *56* (4), 1507−1521.

(33) Song, L. F.; Johnson, P. R.; Elimelech, M. Kinetics of colloid deposition onto heterogeneously charged surfaces in porous media. *Environ. Sci. Technol.* **1994**, *28* (6), 1164−1171.

(34) Johnson, P. R.; Elimelech, M. Dynamics of colloid deposition in porous media: blocking based on random sequential adsorption. *Langmuir* **1995**, *11* (3), 801−812.

(35) Johnson, P. R.; Sun, N.; Elimelech, M. Colloid transport in geochemically heterogeneous porous media: modeling and measurements. *Environ. Sci. Technol.* **1996**, *30* (11), 3284−3293.

(36) Ryan, J. N.; Elimelech, M.; Ard, R. A.; Harvey, R. W.; Johnson, P. R. Bacteriophage PRD1 and silica colloid transport and recovery in

an iron oxide-coated sand aquifer. *Environ. Sci. Technol.* **1999**, *33* (1), 63−73.
(37) Elimelech, M.; Nagai, M.; Ko, C. H.; Ryan, J. N. Relative insignificance of mineral grain zeta potential to colloid transport in geochemically heterogeneous porous media. *Environ. Sci. Technol.* **2000**, *34* (11), 2143−2148.
(38) Abudalo, R. A.; Ryan, J. N.; Harvey, R. W.; Metge, D. W.; Landkamer, L. Influence of organic matter on the transport of *Cryptosporidium parvum* oocysts in a ferric oxyhydroxide-coated quartz sand saturated porous medium. *Water Res.* **2010**, *44* (4), 1104−1113.
(39) Lin, S. H.; Cheng, Y. W.; Bobcombe, Y.; Jones, K. L.; Liu, J.; Wiesner, M. R. Deposition of silver nanoparticles in geochemically heterogeneous porous media: predicting affinity from surface composition analysis. *Environ. Sci. Technol.* **2011**, *45* (12), 5209−5215.
(40) Parks, G. A. Isoelectric points of solid oxides solid hydroxides and aqueous hydroxo complex systems. *Chem. Rev.* **1965**, *65* (2), 177−198.
(41) Zhang, W.; Isaacson, C. W.; Rattanaudompol, U. S.; Powell, T. B.; Bouchard, D. Fullerene nanoparticles exhibit greater retention in freshwater sediment than in model porous media. *Water Res.* **2012**, *46* (9), 2992−3004.
(42) Cheng, C. H.; Lehmann, J.; Engelhard, M. H. Natural oxidation of black carbon in soils: changes in molecular form and surface charge along a climosequence. *Geochim. Cosmochim. Acta* **2008**, *72* (6), 1598−1610.
(43) Wang, D. J.; Bradford, S. A.; Harvey, R. W.; Hao, X. Z.; Zhou, D. M. Transport of ARS-labeled hydroxyapatite nanoparticles in saturated granular media is influenced by surface charge variability even in the presence of humic acid. *J. Hazard. Mater* **2012**, *229*, 170−176.
(44) Wang, D. J.; Zhang, W.; Hao, X. Z.; Zhou, D. M. Transport of biochar particles in saturated granular media: effects of pyrolysis temperature and particle size. *Environ. Sci. Technol.* **2013**, *47* (2), 821−828.
(45) Johnson, P. R. A comparison of streaming and micro-electrophoresis methods for obtaining the zeta potential of granular porous media surfaces. *J. Colloid Interface Sci.* **1999**, *209* (1), 264−267.
(46) Toride, N.; Leij, F. J.; van Genuchten, M. T. The CXTFIT code for estimating transport parameters from laboratiry or field tracer experiments. Version 2.1; U.S. Salinity Laboratory, USDA-ARS: Riverside, CA, 1999.
(47) Pignatello, J. J.; Kwon, S.; Lu, Y. F. Effect of natural organic substances on the surface and adsorptive properties of environmental black carbon (char): attenuation of surface activity by humic and fulvic acids. *Environ. Sci. Technol.* **2006**, *40* (24), 7757−7763.
(48) Polo, M. S.; Utrilla, J. R. Adsorbent-adsorbate interactions in the adsorption of Cd(II) and Hg(II) on ozonized activated carbons. *Environ. Sci. Technol.* **2002**, *36* (17), 3850−3854.
(49) Gu, B. H.; Schmitt, J.; Chen, Z. H.; Liang, L. Y.; Mccarthy, J. F. Adsorption and desorption of natural organic matter on iron oxide: mechanisms and models. *Environ. Sci. Technol.* **1994**, *28* (1), 38−46.
(50) Tipping, E. The adsorption of aquatic humic substances by iron oxides. *Geochim. Cosmochim. Acta* **1981**, *45* (2), 191−199.
(51) Wang, Y. G.; Li, Y. S.; Fortner, J. D.; Hughes, J. B.; Abriola, L. M.; Pennell, K. D. Transport and retention of nanoscale C_{60} aggregates in water-saturated porous media. *Environ. Sci. Technol.* **2008**, *42* (10), 3588−3594.
(52) Tufenkji, N.; Elimelech, M. Breakdown of colloid filtration theory: role of the secondary energy minimum and surface charge heterogeneities. *Langmuir* **2005**, *21* (3), 841−852.
(53) Li, Y. S.; Wang, Y. G.; Pennell, K. D.; Abriola, L. M. Investigation of the transport and deposition of fullerene (C_{60}) nanoparticles in quartz sands under varying flow conditions. *Environ. Sci. Technol.* **2008**, *42* (19), 7174−7180.
(54) Shen, C. Y.; Li, B. G.; Wang, C.; Huang, Y. F.; Jin, Y. Surface roughness effect on deposition of nano- and micro-sized colloids in saturated columns at different solution ionic strengths. *Vadose Zone J.* **2011**, *10* (3), 1071−1081.
(55) Bradford, S. A.; Torkzaban, S.; Leij, F.; Simunek, J.; van Genuchten, M. T. Modeling the coupled effects of pore space geometry and velocity on colloid transport and retention. *Water Resour. Res.* **2009**, *45* (2), doi:10.1029/2008WR007096.
(56) Yao, K. M.; Habibian, M. M.; O'Melia, C. R. Water and waste water filtration: concepts and applications. *Environ. Sci. Technol.* **1971**, *5* (11), 1105−1112.
(57) Bradford, S. A.; Kim, H. N.; Haznedaroglu, B. Z.; Torkzaban, S.; Walker, S. L. Coupled factors influencing concentration-dependent colloid transport and retention in saturated porous media. *Environ. Sci. Technol.* **2009**, *43* (18), 6996−7002.
(58) Tufenkji, N.; Redman, J. A.; Elimelech, M. Interpreting deposition patterns of microbial particles in laboratory-scale column experiments. *Environ. Sci. Technol.* **2003**, *37* (3), 616−623.
(59) Zhang, W.; Niu, J. Z.; Morales, V. L.; Chen, X. C.; Hay, A. G.; Lehmann, J.; Steenhuis, T. S. Transport and retention of biochar particles in porous media: effect of pH, ionic strength, and particle size. *Ecohydrology* **2010**, *3* (4), 497−508.
(60) Bradford, S. A.; Torkzaban, S. Colloid adhesive parameters for chemically heterogeneous porous media. *Langmuir* **2012**, *28* (38), 13643−13651.
(61) Ko, C. H.; Elimelech, M. The "shadow effect" in colloid transport and deposition dynamics in granular porous media: Measurements and mechanisms. *Environ. Sci. Technol.* **2000**, *34* (17), 3681−3689.
(62) Kuhnen, F.; Barmettler, K.; Bhattacharjee, S.; Elimelech, M.; Kretzschmar, R. Transport of iron oxide colloids in packed quartz sand media: monolayer and multilayer deposition. *J. Colloid Interface Sci.* **2000**, *231* (1), 32−41.
(63) El-Badawy, A. M.; Hassan, A. A.; Scheckel, K. G.; Suidan, M.; Tolaymat, T. Key factors controlling the transport of silver nanoparticles in porous media. *Environ. Sci. Technol.* **2013**, *47*, doi:10.1021/es304580r.
(64) Hofmann, A.; Liang, L. Mobilization of colloidal ferrihydrite particles in porous media - an inner-sphere complexation approach. *Geochim. Cosmochim. Acta* **2007**, *71* (24), 5847−5861.
(65) Fritz, G.; Schadler, V.; Willenbacher, N.; Wagner, N. J. Electrosteric stabilization of colloidal dispersions. *Langmuir* **2002**, *18* (16), 6381−6390.
(66) Louie, S. M.; Phenrat, T.; Small, M. J.; Tilton, R. D.; Lowry, G. V. Parameter identifiability in application of soft particle electrokinetic theory to determine polymer and polyelectrolyte coating thicknesses on colloids. *Langmuir* **2012**, *28* (28), 10334−10347.